Vibration isolation characteristic of a modified Gough-Stewart platform with the top platform filled with damping particles

Nazeer Ahmad[1], R Ranganath[2], D Poomani[3], Ashitava Ghosal[4]

[1]Structures Group, U R Rao Satellite Centre, Indian Space Research Organization (ISRO), Bangalore, India, 560017
nazeer@ursc.gov.in
[2]Project Director, SPADEX, U R Rao Satellite Centre, Indian Space Research Organization (ISRO), Bangalore, India, 560017
rrrr@ursc.gov.in
[3]Group Director, Structures Group, U R Rao Satellite Centre, Indian Space Research Organization (ISRO), Bangalore, India, 560017
poomani@ursc.gov.in
[4]Professor, Department of Mechanical Engineering, Indian Institute of Science, Bangalore, 560012
asitava@iisc.ac.in

Abstract. In this paper, we consider a modified Gough-Stewart platform (MGSP) where two groups of three legs meet at two concentric circles on both top and bottom platforms. The geometry of the MGSP is chosen such that all the first six natural frequencies are equal for a typical payload mounted on the top platform. Additionally, in the top platform, made up of an aluminum honeycomb sandwich, the empty cells of the honeycomb core are filled with damping particles (DPs) to introduce passive damping in the system and to limit the resonance responses. A finite element model (FEM) of the MGSP is developed to quantify the performance in terms of frequency response functions (FRF), resonance peaks and the damping introduced by the damping particles. The FEM model of the MGSP is combined with the discrete element model (DEM) of the damping particles to compute the effect of the particles on the overall dynamics and damping behavior of the platform. The effect of DPs on the transfer function is evaluated by solving the equations of motion of the DPs and the FEM model of the MGSP simultaneously. Finally, the FRF between the bottom platform and the mass center of the payload is computed for assessing the effectiveness of DPs, the transfer functions between the base excitation and mass center of the payload with respect to four inputs – sine swept inputs X, Z, θ_X, and θ_Z applied separately at the base of the platform – were computed for 25%, 50%, 75% and 93% fill fractions. The peaks at resonances progressively decrease as the fill fraction was increased. For all the modes, it was seen that the damping introduced by damping particles results in the splitting of the modes and the formation of anti-resonance at resonance peaks. The damping introduced by the particles is more effective in longitudinal direction $||Z/Z||$ where there is a reduction from 25 to 8 with increasing fill fractions from 25% to 93%. The cross-axis transfer functions also

seen to come down from 98 and 10 to 75 and 5 along the X-axis and Y-axis, respectively.

Keywords: Modified Stewart platform, multi-axis vibration control, Particle impact damping.

1 Introduction

The Gough-Stewart platform (GSP) is commonly used in a wide range of applications such as flight simulators, pointing mechanisms, machine tools, force-torque sensors, precision surgery [1, 2], multi-axis vibration isolation [3, 4], etc. The Gough-Stewart platform consists of a movable top platform connected to a base platform by six legs. The length of the legs can be changed to provide a desired position and orientation of the top platform. The design of GSP has been based on various performance criteria such as load-carrying capacity, workspace requirements, range of motion dexterity and isotropy. In the context of kinematics, at an isotropic configuration, the velocity (linear and angular) distribution is a sphere, and the GSP can move with equal `ease' in all directions at these configurations [5], and due to this reason, isotropy is a desired feature in a design. Kinematic isotropy is related to the condition number of a manipulator Jacobian matrix, and several researchers have attempted to design a GSP to obtain kinematic isotropy [6]. In the context of static forces, at an isotropic configuration, the GSP can resist forces and moments equally well in all spatial directions. In the study of statics of the GSP, the so-called force transformation matrix [7, 8] is used instead of the manipulator Jacobian matrix, and again, the goal is to find conditions for which the force transformation matrix has identical singular values. In most of the above work, the researchers discuss various approaches to avoid a basic problem in manipulator Jacobian and force transformation matrices, namely the dimensions of the linear and angular velocity or that of the forces and moments are not the same. In reference [8], the authors derive algebraic conditions for separate force and moment isotropy and claim that it is not possible to obtain identical singular values for both force and moment parts of the force transformation matrices. The dynamic isotropy (DI), the condition of the platform where all the eigenvalues are equal [9], is an important criterion in design of vibration isolator. The dynamic isotropy index is defined as $DII = \omega_{max}/\omega_{min}$ is the ratio, as indicated, of the largest to the smallest natural frequency of the GSP. The geometry and inertia conditions for complete dynamic isotropy (i.e., $DII = 1$) of a GSP is practically not realizable.

In a modified version of the GSP (MGSP), the anchorage points on each platform lie on two circles in contrast to a single circle in the GSP. A set of three legs, which are $120°$ apart, are connected to each circle -- this is based on a concept first presented in [10]. An MGSP with ideal joints and rigid links is known to give the configurations that have complete dynamic isotropy and such an MGSP can be fabricated for real applications. An MGSP with flexural hinges, usually used to avoid friction at the joints, increases the DII or the modal spread. However, the new configurations of the MGSP with flexural joints with $DII = 1$ also exists [11].

In this paper, we assess the vibration isolation performance of a complete dynamic isotropic MGSP with flexural joints, metallic bellows in the leg for stiffness and a top platform made up of an aluminum honeycomb sandwich (see Fig. 1). The empty cells of the core of the honeycomb sandwich are filled with damping particles to introduce damping in the system and thereby limiting the resonance responses. The performance of the MGSP has been quantified in terms of frequency response functions (FRF), resonance peaks and the damping introduced by the damping particles.

A finite element model (FEM) of the MGSP, with the bellows and flexures, top and bottom platforms and connectors were developed in ABAQUS® software. The shell elements S3R were used to mesh the bellows, flexures, and top and bottom platforms. The in-between connectors were model using the solid tetrahedral C3D10 elements[12]. An axis-symmetric payload was modeled using a lumped mass of $m_{pld} = 10$ kg, with in plane inertias $I_{xx}^{pld} = I_{yy}^{pld} = 0.066$ kg-m^2, and out of plane inertia of $I_{zz}^{pld} = 0.1230$ kg-m^2. The inertia values are given with respect to a coordinate system with the origin at the center of mass of the payload and axis are parallel to the global axis in its natural pose. The center of mass (CM) of the payload is assumed to be located at 50 mm above the center of the payload platform. The lumped payload mass was connected to the top platform with beam-type multi-point constraint (MPC). The damping particles were modelled using the discrete element method (DEM) wherein the equations of motion of the particles are obtained using Newton's second law. Whenever the damping particles come into contact with the top platform, the contact forces evolving in the process are modelled using dissipative Hertz contact theory. The FEM model of the MGSP and DEM model of the damping particle are coupled through contact forces and were solved simultaneously using the Runge-Kutta method in the MATLAB® (see details of the FEM-DEM coupled model in [13, 14]). Finally, the FRF between the mass center of the payload and the bottom platform was computed for assessing the effectiveness of DPs.

2 Mathematical formulations

The governing finite element equations of the MGSP can be written as

$$\mathbf{M}\ddot{\boldsymbol{\chi}} + \mathbf{C}\dot{\boldsymbol{\chi}} + \mathbf{K}\boldsymbol{\chi} = \mathbf{f}^e + \mathbf{f}^d \tag{1}$$

where $\mathbf{M}$, $\mathbf{C}$ and $\mathbf{K}$ are mass, damping and stiffness matrices respectively. $\mathbf{f}^d$ represents the particle damping forces and $\mathbf{f}^e$ is the external excitation forces. The assembled displacement vector $\boldsymbol{\chi}$ consists of the nodal displacement vectors. The $\boldsymbol{\chi}$ is arranged such that all the nodal displacements of the bottom platform are in the vector $\boldsymbol{\chi}_b$ and remaining nodal displacements are in the vector $\boldsymbol{\chi}_s$ so that $\boldsymbol{\chi} = [\boldsymbol{\chi}_s, \boldsymbol{\chi}_b]$. Accordingly, the other matrices in Eq. 1 can be partitioned as [15]

$$\begin{bmatrix} \mathbf{M}_{ss} & \mathbf{M}_{sb} \\ \mathbf{M}_{bs} & \mathbf{M}_{bb} \end{bmatrix} \begin{Bmatrix} \ddot{\boldsymbol{\chi}}_s \\ \ddot{\boldsymbol{\chi}}_b \end{Bmatrix} + \begin{bmatrix} \mathbf{C}_{ss} & \mathbf{C}_{sb} \\ \mathbf{C}_{bs} & \mathbf{C}_{bb} \end{bmatrix} \begin{Bmatrix} \dot{\boldsymbol{\chi}}_s \\ \dot{\boldsymbol{\chi}}_b \end{Bmatrix} + \begin{bmatrix} \mathbf{K}_{ss} & \mathbf{K}_{sb} \\ \mathbf{K}_{bs} & \mathbf{K}_{bb} \end{bmatrix} \begin{Bmatrix} \boldsymbol{\chi}_s \\ \boldsymbol{\chi}_b \end{Bmatrix} = \begin{Bmatrix} \mathbf{f}_s^e \\ \mathbf{f}_b^e \end{Bmatrix} + \begin{Bmatrix} \mathbf{f}_s^d \\ \mathbf{f}_b^d \end{Bmatrix} \tag{2}$$

the base acceleration is enforced on the $\boldsymbol{\chi}_b$ degree-of-freedoms (DOFs). The first part of Eq. 2 is given as

$$\mathbf{M}_{ss}\ddot{\boldsymbol{\chi}}_s + \mathbf{C}_{ss}\dot{\boldsymbol{\chi}}_s + \mathbf{K}_{ss}\boldsymbol{\chi}_s = \mathbf{f}_s^d + \mathbf{f}_s^e - (\mathbf{M}_{sb}\ddot{\boldsymbol{\chi}}_b + \mathbf{C}_{sb}\dot{\boldsymbol{\chi}}_b + \mathbf{K}_{sb}\boldsymbol{\chi}_b) \tag{3}$$

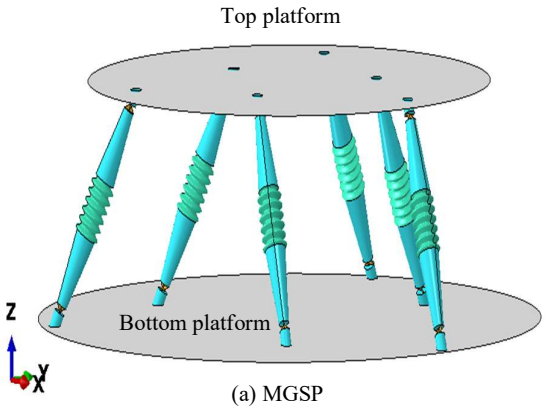

(a) MGSP

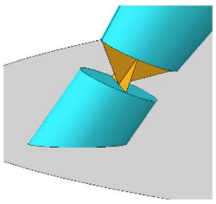

(b) Cross blade flexure

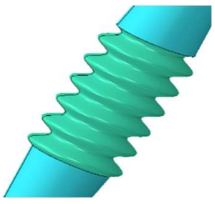

(c) Metallic Bellow

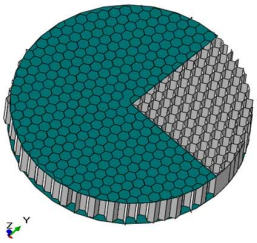

(d) Honeycomb top platform

Fig. 1. A modified Gough-Stewart platform (MGSP) with the main components

Using the transformation $\boldsymbol{\chi}_s = \boldsymbol{\Phi}_s\mathbf{q}_s$, where the modal matrix $\boldsymbol{\Phi}_s$ is obtained from the eigenvalue problem: $(\mathbf{K}_{ss} + \boldsymbol{\Omega}_s^2\mathbf{M}_{ss})\boldsymbol{\Phi}_s = 0$ and invoking the orthogonality relation with respect to mass and stiffness matrix and assuming viscous damping i.e. $\mathbf{C}_{ib}\dot{\boldsymbol{\chi}}_b = \mathbf{0}$, Eq. 3 can be written as.

$$\ddot{\mathbf{q}} + 2\zeta\boldsymbol{\Omega}\dot{\mathbf{q}} + \boldsymbol{\Omega}^2\mathbf{q} = \boldsymbol{\Phi}^T(\mathbf{f}_s^d + \mathbf{f}_s^e) - \boldsymbol{\Phi}^T(\mathbf{M}_{sb}\ddot{\boldsymbol{\chi}}_b + \mathbf{K}_{sb}\boldsymbol{\chi}_b) \tag{4}$$

In Eq. 3 the damping particle force $\mathbf{f}_s^d$ is related to the motions of damping particles impacting against the walls of the honeycomb cell. Let the damping particle i in cells of honeycomb be in contact with n_1 number of neighboring particles and n_2 points with cell walls, then the equations of motion can be written as

$$m_i\ddot{\mathbf{P}}_i = -m_i\mathbf{g} + \sum_{j=1}^{n_1}\mathbf{f}_{ij} + \sum_{w=1}^{n_2}\mathbf{f}_{iw} \tag{5}$$

$$\mathbf{I}\ddot{\boldsymbol{\Theta}}_i = \sum_{j=1}^{n_1}\left(r_i - \frac{\delta_{ij}}{2}\right)\mathbf{n}_{ij} \times \mathbf{f}_{ij} + \sum_{w=1}^{n_2}(r_i - \delta_{iw}))\mathbf{n}_{iw} \times \mathbf{f}_{iw} \tag{6}$$

where m_i and $\mathbf{I}$ are the mass and inertia matrix, respectively, of the particle i while $\mathbf{P}_i$ is the position vector and $\boldsymbol{\Theta}_i$ is the angular displacement. $\mathbf{g}$, r_i, δ_{ij} and $\mathbf{f}_{ij}$ represent acceleration due to gravity, radius of the damping particle i, local indention and contact force between particles i and j, respectively. The Eqs. 4-6 are coupled and must be solved together. For a base excitation problem, it is assumed that the base is excited with a known signal, and thus $\ddot{\boldsymbol{\chi}}_b$ and $\boldsymbol{\chi}_b$ is a known *priori*. The modal vector and natural frequencies along with the sub-matrices appearing in Eq. 4 were obtained from the FEM model. The integration of Eqs. 4-6 was carried out in MATLAB® using a Runge-Kutta method (ODE-45).

3 Numerical simulations

The MGSP is excited at the base platform by a sine sweep input signal of constant magnitude and frequency ranging from 5 Hz to 300 Hz. The input can be written mathematically as

$$u = \sin\left(2\pi\left(f_s + \frac{(f_{end}-f_s)t}{2t_{end}}\right)t\right) \tag{7}$$

where f_s, f_{end} and t_{end} are respectively, the start frequency, the end frequency and the sweep duration. The input signal u can be a linear or angular displacement. A slice of the normalized input signal is given in Fig. 2.

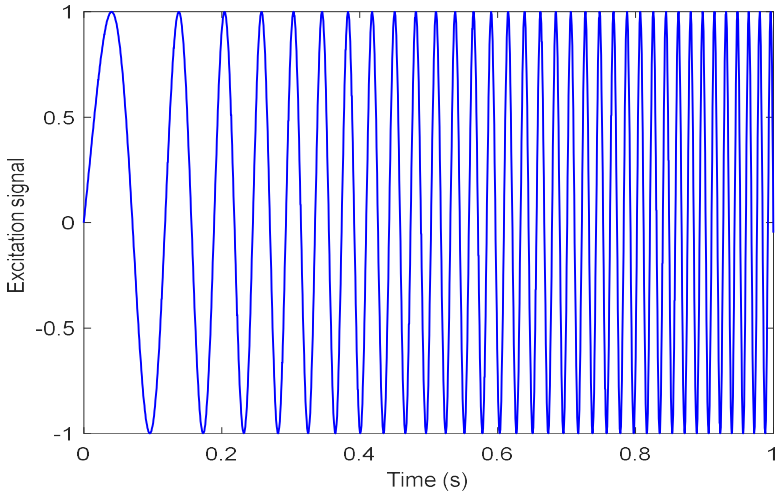

Fig. 2. Input swept sine signal

The input displacement swept sine signal in X, Z, θ_X and θ_Z directions were applied at the center of the base platform separately, and the output response at the mass center of

the payload was computed using the coupled equations of motion. Transfer functions described in the following sections were obtained from the time domain signals using the *tfestimate* function from the signal processing toolbox of MATLAB® for the various amounts of damping particles filled in the cells of the top platform.

3.1 Effect of fill fraction on FRFs with longitudinal axis (Z-axis) input

Fig. 3-5 show the transfer functions between the displacement sine swept input applied in the longitudinal direction (Z-axis) and the displacement responses in X-axis, Y-axis and Z-axis, respectively. The four cases considered are 25%, 50%, 75% and 93% fill fractions -- the fill fraction is defined as the ratio of the filled volume of the honeycomb cell to the total volume of the cell. The damping particles are uniformly filled in the empty cells of the honeycomb core of the top platform. A 25% fill fraction implies that all the cells of the top platform are filled to 25% of the thickness. The amplification at resonance in the longitudinal direction is progressively decreasing -- as seen in Fig.3 that the amplification reduces from 25 to 8 as the fill fraction is increased from 25% to 93%. The maximum reduction in the response at resonance happens when the fill fraction is between 85% to 93% (when the fill fraction is near 100%, the damping particles do not have space for motion and hence a lesser number of collisions and subsequently less dissipation of energy take place). It can be seen that the longitudinal mode at 30.43 Hz has split into two modes, and there is an anti-resonance at that frequency after the introduction of damping particles. The cross-axis amplifications at resonance have reduced, but the reduction is not as much as along the Z-axis. The $||X/Z||$ amplifications have come down from 98 to 75; and $||Y/Z||$ amplifications have come down from 10 to 5 when the fill fractions were varied from the 25% to 93%. It can be seen there is also splitting of modes and introduction of two anti-resonances in the isolation region, which is advantageous.

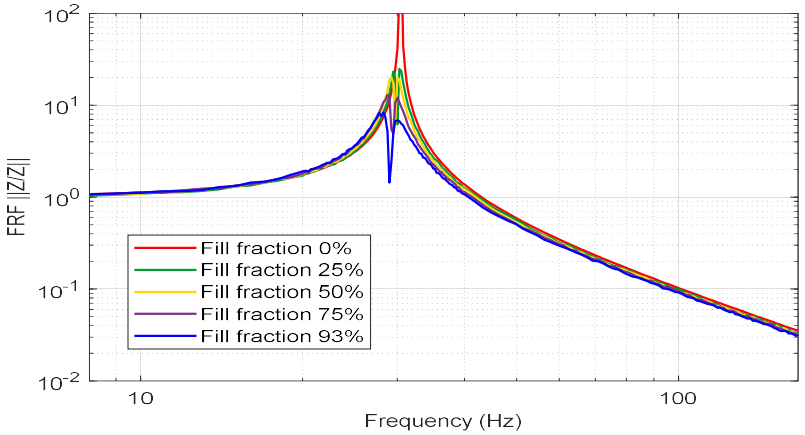

Fig. 3. Transfer function between Z-axis input and Z-axis output

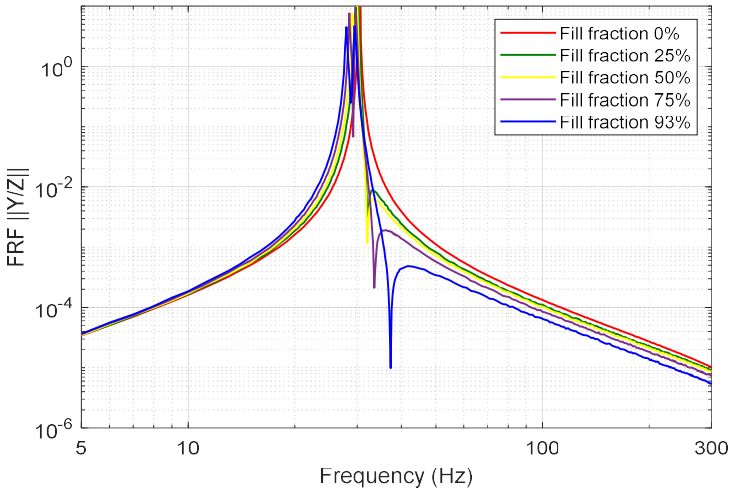

Fig. 4. Transfer function between Z-axis input and Y-axis output

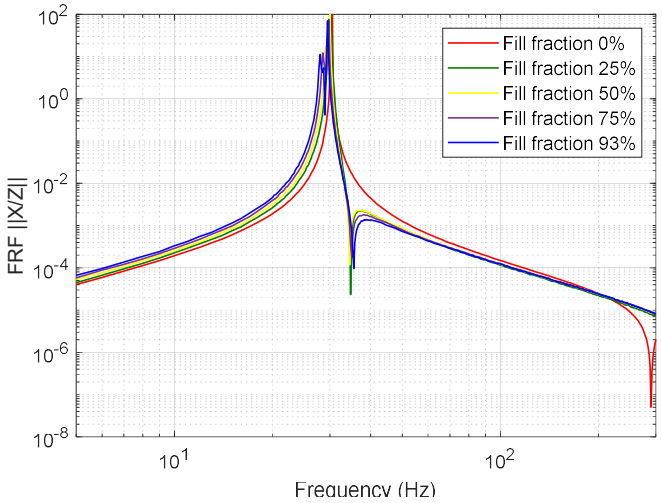

Fig. 5. Transfer function between Z-axis input and X-axis output

3.2 Effect of fill fraction on FRFs with lateral axis (X-axis) input

The transfer functions between the displacement sine swept input applied along the X-axis at the base platform and the output displacement responses in the X-axis, Y-axis and Z-axis at the mass center of the payload, respectively, are shown in Fig. 6-8. The

four cases considered for the damping particles are 25%, 50%, 75% and 93% fill fractions. The resonance responses for in X-axis and Y-axis are mildly reduced, split and shifted for X-axis excitation. The $||X/X||$ FRFs reduced from an amplification of 164 at 25% fill fraction to 130 at 93%. The cross-axis FRFs ||Y/X|| and ||Z/X|| shows a marginal improvement in the damping at 93% fill fraction. The undamped to the damped reduction in amplitudes is from 14 to 8.8 and from 9.9 to 7.5 for the ||Y/X|| and ||Z/X|| transfer function, respectively. The resonance peak amplifications are seen to increase as the fill fraction is increased from 25% to 50%. The likely reason for this could be the in-phase momentum transfer between the top platform and DPs.

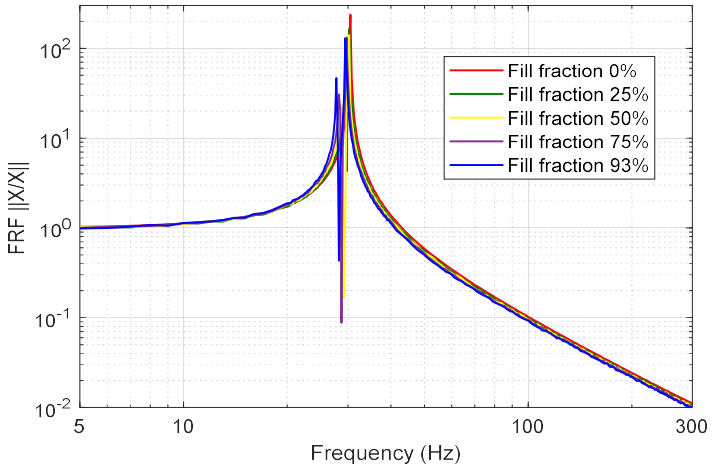

Fig. 6. Transfer function between X-axis input and X-axis output

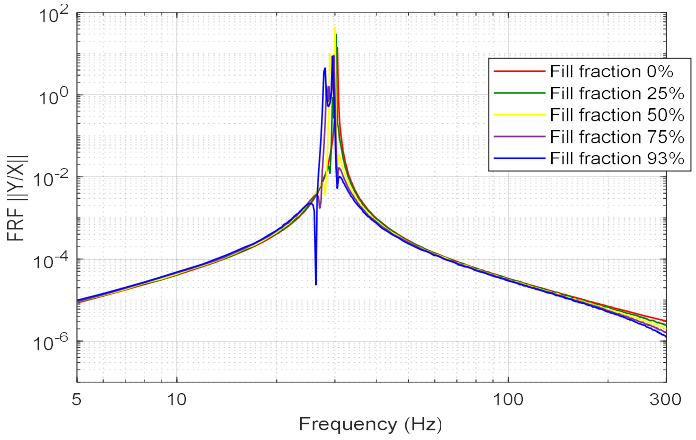

Fig. 7. Transfer function between X-axis input and Y-axis output

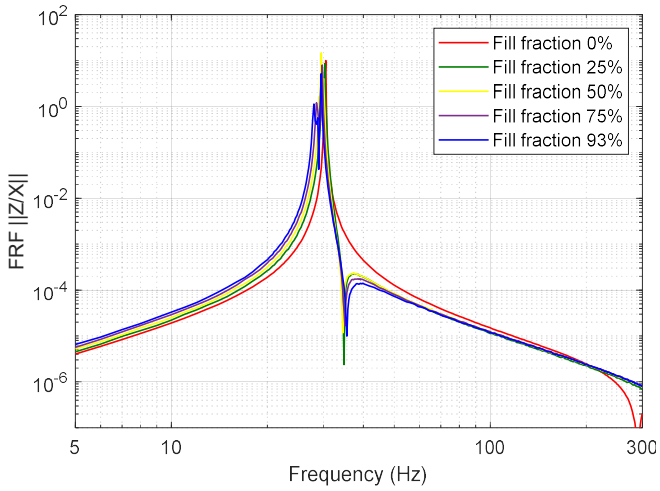

Fig. 8. Transfer function between X-axis input and Z-axis output

3.3 Effect of fill fraction on FRFs with θ_X input excitation

Figs. 9-11 show the transfer functions between the input angular displacement θ_X applied to the base platform and the angular displacement responses θ_X, θ_Y and θ_Z, respectively, at the top platform. Unlike the translational cases where the input to the cross translational and rotational directions was set zero, in this case, the Z-axis translation of the base plate was kept free to allow the rotation about the X-axis. Again, the transfer functions for the four fill fractions of 25%, 50%, 75% and 93% were considered. As in the previous results, splitting of mode with a mild reduction in magnitude was observed. The reduction in responses θ_X, and θ_Y are more in comparison to the θ_Z. The FRFs $||\theta_X/\theta_X||$ and $||\theta_Y/\theta_X||$ comes down from 287 and 73 to 150 and 42, respectively, while the reduction in $||\theta_Z/\theta_X||$ is from 40.6 to 32. The reason for the 1.9 times and 1.7 times reduction in $||\theta_X/\theta_X||$ and $||\theta_Y/\theta_X||$ respectively is due to the movement of particles at the edge of the top platform due to rotation of the platform about θ_X and θ_Y axis which gives motion in Z-axis. The θ_Y input behavior is expected to be similar to θ_X.

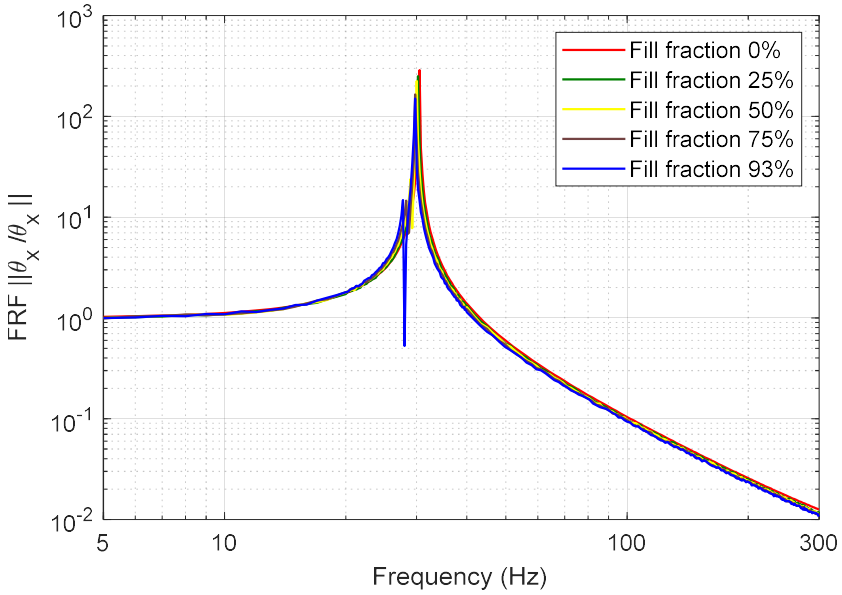

Fig. 9. Transfer function between θ_X input and θ_X output

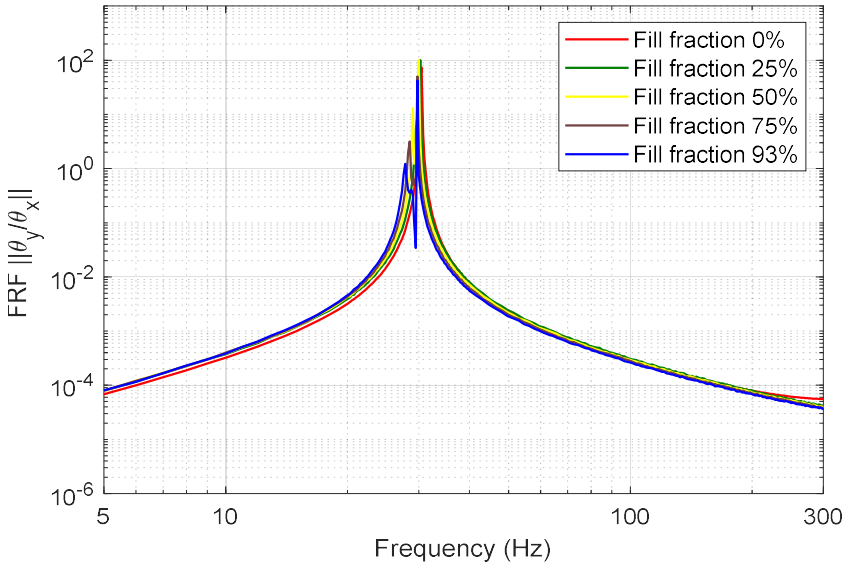

Fig. 10. Transfer function between θ_x input and θ_Y output

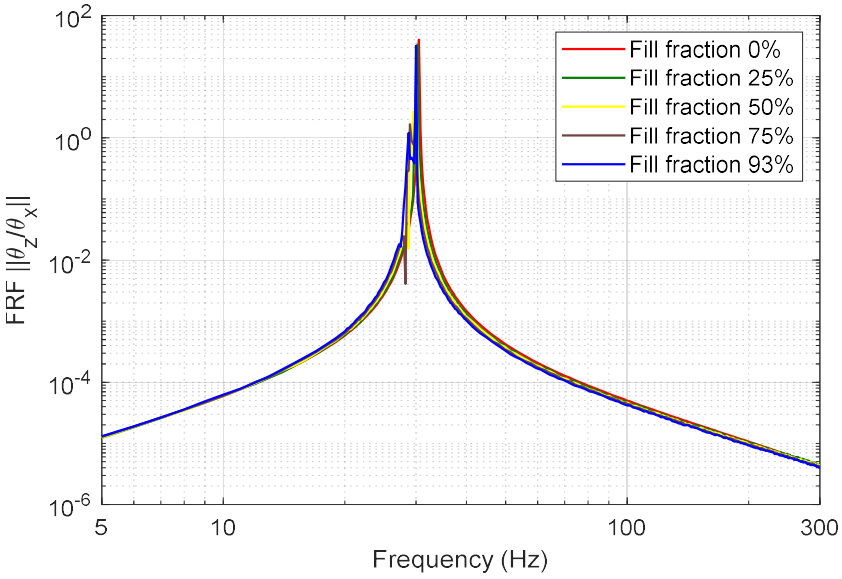

Fig. 11. Transfer function between θ_x input and θ_z output

3.4 Effect of fill fraction on FRFs with θ_Z input excitation

The transfer functions between the torsional input θ_Z and responses θ_X, θ_Y and θ_Z are shown in Figs. 12-14, respectively. As expected, there is a significant reduction in resonance amplitude in cross-axis FRFs while it is negligible in the θ_Z direction. The FRF $||\theta_X/\theta_Z||$ reduces from 201 to 109 while $||\theta_Y/\theta_Z||$ has come down to 140 from 251. The reason for the reduction is that the rotation of the top plate about θ_X and θ_Y axis involves significant motion of the cell at the outer boundary in Z-direction. Since the particle can move in Z-directions, collisions would lead to increased dissipation. In the torsional rotation of the top deck, there is not much scope for the movement of damping particles, and hence the impact is negligible. The θ_X and θ_Y rotations result in motion in Z-direction at the location away from the axis of rotations, and because of that the DPs move in the cells colliding and rubbing resulting in the improvement of the damping behavior and thus the reduction in the cross-axis resonance amplitudes.

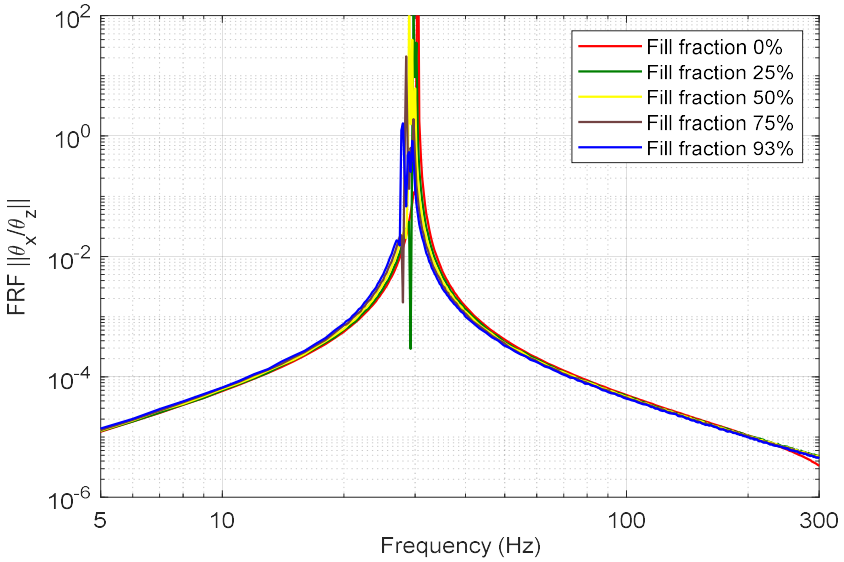

Fig. 12. Transfer function between θ_Z input and θ_X output

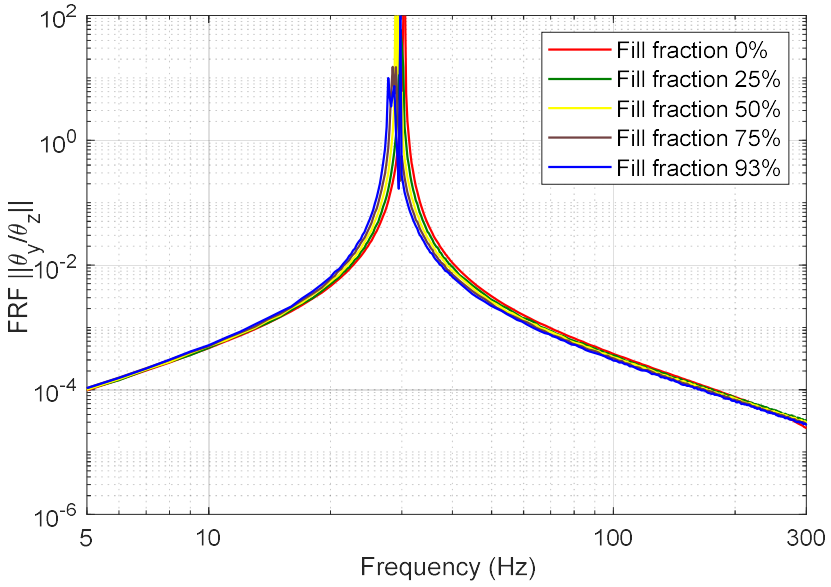

Fig. 13. Transfer function between θ_Z input and θ_Y output

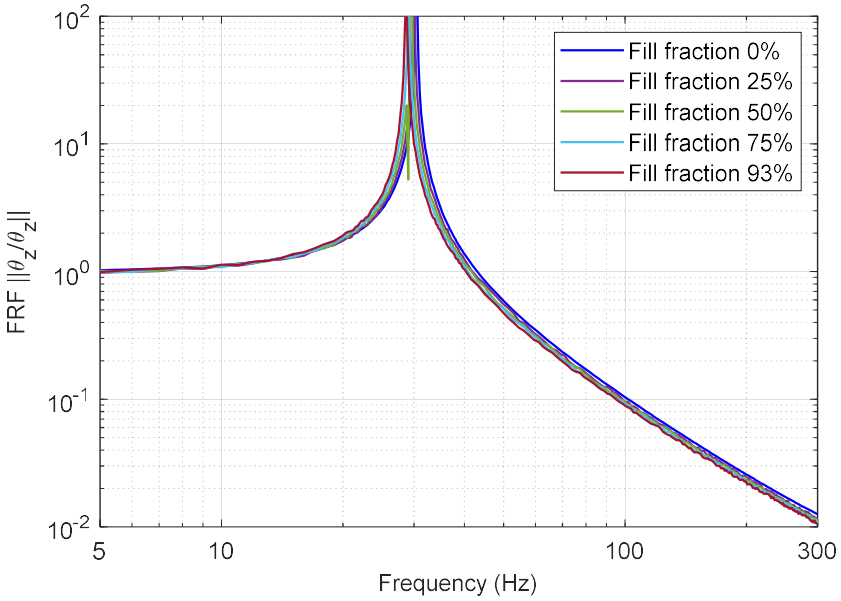

Fig. 14. Transfer function between θ_Z input and θ_Z output

4 Conclusions

The transfer functions between the base excitation and mass center of the payload mounted on the top platform of the MGSP, using the couple DEM-FEM equations of motion of the MGSP, were computed. The cells of the honeycomb core of the top platform were filled with damping particles. The transfer functions FRFs with respect to four inputs, swept sine inputs X, Z, θ_x, and θ_Z applied separately at the base of the platform, were computed for 25%, 50%, 75% and 93% fill fractions. The behavior with respect to inputs Y and θ_Y are nearly similar to X and θ_x. The peaks at resonances progressively decreased as the fill fraction was increased. For all the modes, it was seen that the damping introduced by damping particles results in the splitting of the modes and the formation of anti-resonance at the frequency of un-damped resonance. As the MGSP without damping particles have all the modes at the same frequency, the splitting at resonance happens due to the presence of close by modes resulting from the addition of mass of the damping particle in the system. The splitting of modes and formation of anti-resonance is advantageous as it reduces the amplification. The damping introduced by the particles is more effective in longitudinal direction $||Z/Z||$ where there is a reduction from 25 to 8 with increasing fill fractions from 25% to 93%. The cross-axis transfer functions also come down from 98 and 10 to 75 and 5 along the X-axis and Y-axis, respectively. The reduction in most of the cross-axis transfer functions was seen. The ratio of the damped and undamped magnitude of the FRFs for θ_X input is

$[1.9, 1.7, 1.2\ ]$ and θ_Z input is $[1.8, 1.7, 1.03]$ for θ_X, θ_Y and θ_Z axis. However, it is not effective in limiting the resonance at torsional mode $||\theta_Z/\theta_Z||$. The magnitude of the FRF $||\theta_Z/\theta_Z||$ at resonance with damping particle and without damping particle is 268.5 and 298.5, respectively.

5 References

1. J. P. Merlet, Parallel Robots, 2nd ed. Netherlands: Springer Netherlands, 2012.
2. P. Mukherjee, B. Dasgupta, and A. K. Mallik, "Dynamic stability index and vibration analysis of a flexible Stewart platform," Journal of Sound and Vibration, vol. 307, no. 3-5, pp. 495-512, 2007. DOI: 10.1016/j.jsv.2007.05.036
3. R. B. A. Shyam, N. Ahmad, R. Ranganath, and A. Ghosal, "Design of a dynamically isotropic Stewart-Gough platform for passive micro-vibration isolation in spacecraft using optimization," Journal of Spacecraft Technology, vol. 30, no. 2, pp. 1-8, December 2019.
4. M. Furqan, M. Suhaib, and N. Ahmad, "Dynamic analysis of six-axis Stewart platform using flexible joints," International Journal of Mechanisms and Robotic Systems, vol. 4, no. 3, pp. 214-233, 2018. DOI: 10.1504/ijmrs.2018.095965
5. C. A. Klein and T. A. Miklos, "Spatial robotic isotropy," The International Journal of Robotics Research, vol. 10, no. 4, pp. 426-437, 1991.
6. K. E. Zanganeh and J. Angeles, "Kinematic isotropy and the optimum design of parallel manipulators," The International Journal of Robotics Research, vol. 16, no. 2, pp. 185-197, 1997.
7. K. Tsai and K. Huang, "The design of isotropic 6-DOF parallel manipulators using isotropy generators," Mechanism and Machine Theory, vol. 38, no. 11, pp. 1199-1214, 2003.
8. S. Bandyopadhyay and A. Ghosal, "An algebraic formulation of static isotropy and design of statically isotropic 6–6 Stewart platform manipulators," Mechanism and Machine Theory, vol. 44, no. 7, pp. 1360-1370, 2009.
9. B. Afzali-Far and P. Lidström, "Analytical index of dynamic isotropy and its application to hexapods," Precision Engineering, vol. 52, pp. 242-248, 2018. DOI: 10.1016/j.precisioneng.2018.01.001
10. Z. Tong, J. He, H. Jiang, and G. Duan, "Locally dynamic isotropy of modified symmetric Gough-Stewart parallel micromanipulators," in 13th World Congress in Mechanism and Machine Science, Guanajuato, México, 2011, pp. 19-25.
11. N. Ahmad, "Vibration mitigation in spacecraft components using Stewart platform and particle impact damping," PhD Thesis, Department of Mechanical Engineering, Indian Institute of Science, Bangalore, 2021.
12. Abaqus-6.13, "Abaqus/CAE User's manual," Available: www.simulia.com.
13. N. Ahmad, R. Ranganath, and A. Ghosal, "Modeling of the coupled dynamics of damping particles filled in the cells of a honeycomb sandwich plate and experimental validation," Journal of Vibration and Control, vol. 25, no. 11, pp. 1706-1719, 2019. DOI: 10.1177/1077546319837584
14. N. Ahmad, R. Ranganath, and A. Ghosal, "Modeling and experimental study of a honeycomb beam filled with damping particles," Journal of Sound and Vibration, vol. 391, pp. 20-34, 2017/03/17/ 2017. DOI: doi.org/10.1016/j.jsv.2016.11.011
15. J. Wijker, Mechanical Vibrations in Spacecraft Design. New York: Springer-Verlag Berlin Heidelberg, 2004.